Tagging of Protonated Ala-Tyr and Tyr-Ala by Crown Ether Prevents Direct Hydrogen Loss and Proton Mobility after Photoexcitation: Importance for Gas-Phase Absorption Spectra, Dissociation Lifetimes, and Channels

Jean Ann Wyer,* Anneli Ehlerding, Henning Zettergren, Maj-Britt S. Kirketerp, and Steen Brøndsted Nielsen

Department of Physics and Astronomy, Aarhus University, Ny Munkegade, DK-8000 Aarhus C, Denmark

Received: May 1, 2009; Revised Manuscript Received: July 9, 2009

Photodissociation of protonated Tyr, Ala-Tyr, Tyr-Ala (Ala = alanine, Tyr = tyrosine), and their complexes with 18-crown-6-ether (CE) was performed in an electrostatic ion storage ring using a tunable laser system. While the three bare ions all absorb strongly at 222 nm, absorption at higher wavelengths was barely visible from sampling the neutrals formed in delayed dissociation. A band at 270 nm was introduced, however, as a consequence of CE attachment to the bare ions. To understand the difference between bare ions and complexes, electronically excited states are considered: The initially reached $\pi\pi^*$ state on phenol couples with the dissociative $\pi\sigma^*$ state on ammonium, which leads to direct hydrogen loss. Cold radical cations are formed that at high wavelengths do not have enough energy for further dissociation. Excitation within the 222-nm band on the other hand leads to delayed dissociation of stored radical cations that is monitored in the present setup. The $\pi\sigma^*$ state moves out of the spectral region upon CE attachment, and instead statistical dissociation is sampled on the microsecond to millisecond time scale at all wavelengths. Our data demonstrate the strength of using supramolecular complexes for action spectroscopy experiments to prevent erroneous spectra as a result of undesired dissociation (H loss) from electronically excited states. The gas-phase absorption spectra firmly establish the perturbations of the phenol electronic structure by a water solvent: The 270-nm band red shifts by ~5 nm, whereas the 222-nm band changes by ~3 nm. Both transitions occur in the phenol group. These results may be useful for protein dynamics experiments that rely on electronic excitations. Product ion mass spectra of $[Tyr + H]^+$, $[Ala\text{-}Tyr + H]^+$, $[Tyr\text{-}Ala + H]^+$, $[Ala\text{-}Tyr + H]^+$(CE), and $[Tyr\text{-}Ala + H]^+$(CE) significantly depend on the excitation wavelength from 210 to 310 nm and on whether the ionizing proton is mobile or not.

Introduction

Electronic absorption by biochromophore ions in vacuo has become a topic of high current interest since the first gas-phase absorption spectrum of the isolated green fluorescent protein (GFP) chromophore anion was published in 2001.[1] A comparison with the protein absorption spectrum revealed that the best way to approximate the environment of the buried chromophore was to take it as being a vacuum. On the other hand, the absorption was completely different in bulk water solution due to charge localization by the polar water molecules. Other work has concentrated on protonated Schiff-base retinal,[2,3] which is the chromophore responsible for vision. Here, the amino acid residues in the neighborhood of the chromophore play a significant role in color tuning, which allows us to perceive light from red to blue. Metalloporphyrins are another class of highly important biochromophores. Recently, the Soret marker band of isolated Fe(III)-heme cations was reported by Lykkegaard et al.[4] along with the spectral changes upon histidine ligation. If four-center ferric heme exists inside a hydrophobic pocket or crevice of a heme protein, its absorption should resemble that of the isolated species. The gas-phase absorption spectra serve a dual purpose as they are also used extensively to benchmark theoretical models.[5−13]

Gas-phase absorption spectroscopy on macromolecular ions has been made possible in our laboratory from the combination of an electrospray ion source, an electrostatic ion storage ring, and pulsed lasers.[14,15] In the ring, the ions are photoexcited, and their lifetimes are measured with respect to dissociation. The problem with finite sampling intervals encountered in finite length time-of-flight instruments (kinetic shifts) is circumvented, and the actual number of photoexcited ions at all wavelengths may be obtained from fits to exponential decays of the ions. A new implementation of pulsed power supplies for all ring elements has allowed for time-dependent photodissociation mass spectroscopy on the microsecond to millisecond time scale,[14−16] which is not routinely done with other instruments. While the mass resolution is poor (about 100), it is in most cases high enough to determine the dissociation channels and their time dependence.

In the present work, the focus is on the photophysics and photodissociation of isolated peptide cations. Knowledge on how the absorption of amino acids and peptides changes as the environment varies is useful for optical probing and labeling and for the choice of wavelength for UV resonance Raman experiments on proteins.[17] Interestingly, recent work on silver trimer−dipeptide bioconjugates showed that peptide absorption was enhanced and extended to a larger range of wavelengths due to Ag_3^+ complexation.[18]

Peptides containing the aromatic amino acid tyrosine absorb in the UV and are photodissociated in mass spectroscopy

* To whom correspondence should be addressed. E-mail: jeanwyer@phys.au.dk.

10.1021/jp904053d CCC: $40.75
Published on Web 07/29/2009

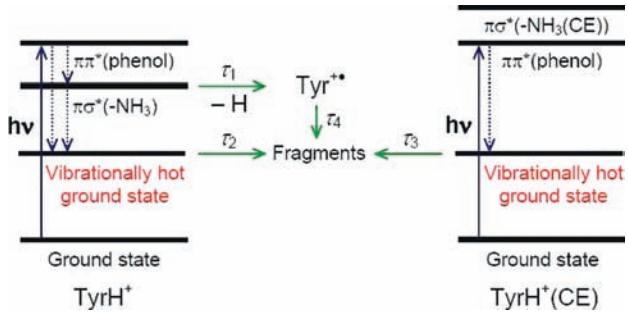

Figure 1. Simplified state level diagrams including some important states. After photoexcitation of protonated tyrosine ($\pi\pi^*$ transition in the phenol group), internal conversion (IC) occurs either back to the electronic ground state (GS) or to a charge-transfer (CT) state located on ammonium, cf. dashed arrows. In the former case a vibrationally excited ion that decays statistically is formed. In the latter case, hydrogen loss is in competition with IC to the GS. The CT state is not accessible in the supramolecular complex between protonated tyrosine and 18-crown-6 ether, and the pathway is IC back to the GS followed by statistical dissociation. The relationship between the time constants is as follows: $\tau_1 \ll \tau_2 \ll \tau_3 < \tau_4$. τ_4 represents a broad range of time constants.

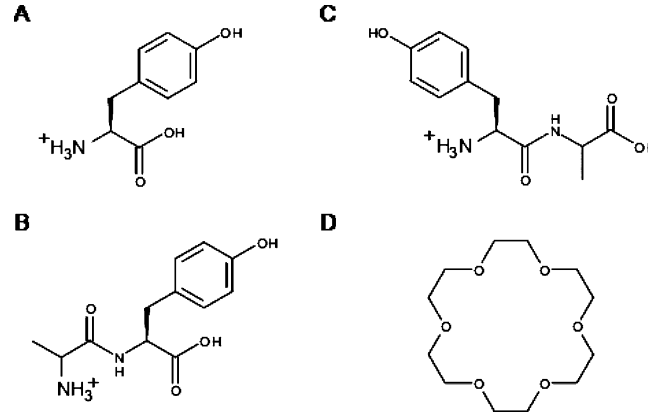

Figure 2. Structures of (A) $[Tyr + H]^+$, (B) $[Ala\text{-}Tyr + H]^+$, (C) $[Tyr\text{-}Ala + H]^+$, and (D) 18-crown-6 ether.

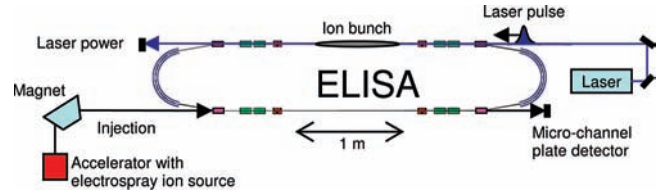

Figure 3. Schematic of the ELISA electrostatic storage ring in combination with a laser system. The photofragment yield was obtained as a function of wavelength from the signal of neutrals hitting the detector.

experiments with conventional lasers.[19−22] If the initial energy is known, the excitation energy after photon absorption is well-defined. This offers an advantage over methods using collisional excitation.[23] Many previous experiments on tyrosine and tyrosine-containing peptides have been completed in conjunction with another biologically significant amino acid, tryptophan (Trp).[18−22,24−35] Subsequent to UV excitation of the indole aromatic ring in tryptophan to a $\pi\pi^*$ state, several dissociation pathways are available.[36] In one such dissociation channel, the $\pi\pi^*$ state couples with a lower lying repulsive $\pi\sigma^*(NH_3)$ state, located on the ammonium group leading to dissociation along the NH coordinate. The energy distribution of the remaining radical cation $Trp^{+\bullet}$ is broad as the kinetic energy range of the ejected hydrogen atom is large. Consecutive dissociation occurs on a microsecond to millisecond time scale.[25,37,38] For protonated tyrosine, however, the NH fragmentation pathway is less accessible after 266-nm photoexcitation as the $\pi\sigma^*(NH_3)$ state is situated at a higher energy (3.4 eV for Trp vs 4.0 eV for Tyr).[25] Previous work has shown that the energy of the $\pi\sigma^*(NH_3)$ state is higher when 18-crown-6 ether (CE) is attached to the ammonium group, rendering the state inaccessible after 260-nm excitation (see Figure 1).[39,40] The size of the chosen crown ether is optimum for the formation of three hydrogen bonds with ammonium.[41−43] Tagging of peptide ammonium groups by crown ether impacts not only the photophysics but, as we will show, also the dissociation channels.

Here we have explored the photophysics of protonated Ala-Tyr, Tyr-Ala (Ala = alanine and Tyr = tyrosine), and their complexes with CE isolated in vacuo (Figure 2), and whether or not water has an influence on the electronic transition energies. Lifetime measurements, absorption spectra, and photodissociation mass spectra are presented, and the results compared to those for protonated Tyr. $[Tyr + H]^+$ has earlier been studied in detail by Kang et al.[25] for 266-nm photoexcitation, but we have extended the excitation region down to 210 nm, accessing a different electronic transition.

Experimental Section

All compounds were purchased from Sigma-Aldrich.

Gas-Phase Experiments. Experiments were carried out at the electrostatic ion storage ring in Aarhus (ELISA) (see Figure 3).[14,15] Electrospray ionization was used to produce the ions which were subsequently accumulated in a 22-pole ion trap and thermally equilibrated by collisions with a helium buffer gas therein. The ions were accelerated as an ion bunch to kinetic energies of 22 keV, and a bending magnet was used to select the appropriate ions. Following injection into the ring, the ions were stored for about 40 ms before being irradiated by a nanosecond light pulse from a tunable EKSPLA laser. This is an Nd:YAG laser where the third harmonic (355 nm) pumps an optical parametric oscillator (OPO). The visible output from this OPO is frequency doubled in a crystal providing UV light. The repetition rate of the experiment was 10 Hz. Dissociation was a result of one photon absorption. Lifetimes were obtained from measurements of the yield of neutrals hitting the micro-channel plate (MCP) detector located at the end of the straight section opposite to the side where photoexcitation was performed.

In separate experiments, the ring voltages were changed at a particular time after photoexcitation to store product ions with the appropriate kinetic energy. This product ion mass spectrometry was possible as ELISA has been equipped with pulsed power supplies of microsecond response times.[14−16] After a specific number of revolutions, the product ions were dumped into the MCP detector. Ions with a lower kinetic energy were evident when a low number of revolutions was used, while ions with a higher kinetic energy were indistinguishable in such a case as ELISA preferentially stores ions with a larger kinetic energy. Ions with a higher kinetic energy were resolved when a higher number of revolutions were undertaken prior to dumping on the detector. Ions with a lower kinetic energy were, however, not evident on such spectra. To increase the resolution, a beam scraper was put in on one side of the ring. The signal from the detector as a function of the scaling of the ring voltages provided the product ion mass spectrum. The pressure in the ring was of the order of 10^{-11} mbar, which set an upper limit of seconds on the storage time.

Solution-Phase Experiments. Solution-phase absorption spectroscopy experiments were carried out using a Thermo

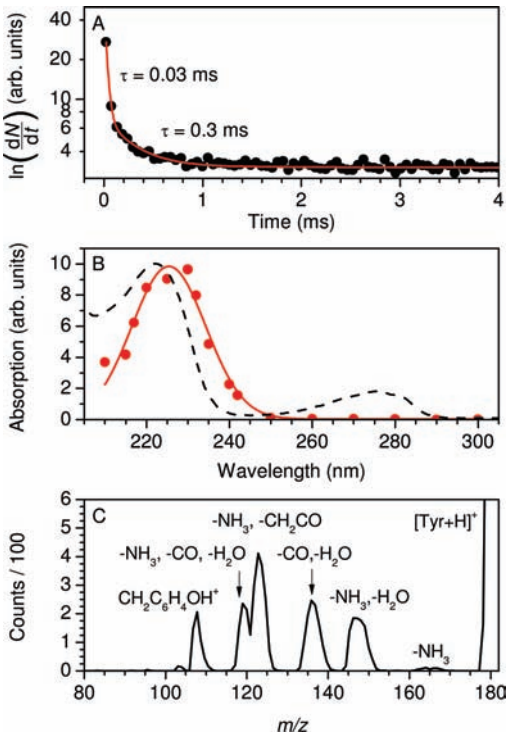

Figure 4. (A) Time spectrum of $[Tyr + H]^+$ (*m/z* 182) after 220-nm photoexcitation. The solid curve is a fit of three exponentials to the data. It was found that the lifetimes associated with the first two exponentials were 0.03 and 0.3 ms, and the lifetime associated with the exponential corresponding to the background decay was 0.4 s. (B) Absorption spectrum of $[Tyr + H]^+$ in vacuo. A Gaussian fit to the data (red points) is shown as a solid line. The solution-phase absorption spectrum is shown as a dashed line. (C) Photodissociation mass spectrum of $[Tyr + H]^+$ after 220-nm photoexcitation.

Spectronic heλios α instrument. Compounds were dissolved in water and spectra recorded from 190 to 325 nm.

Results and Discussion

Protonated Tyrosine. Our initial experiments focused on the decay of $[Tyr + H]^+$ after photoexcitation. A sample time spectrum of $[Tyr + H]^+$ after photoexcitation, measured by detecting the neutral fragments on one side of the ring, is shown in Figure 4A. These were produced between 27 and 45 μs after photoexcitation in the first instance and then after successive rotations in the ring. In order to fit the data, it was found that three separate exponentials were required. The fastest decay had time constants of the order of 10^{-2} ms. The next decay had time constants of the order of 10^{-1} ms, and while it is possible that this decay is due to excitation into a triplet state, it is more likely a tail associated with the first decay due to a broad energy distribution.[38] The more exponentials that are required, the broader the internal energy distribution; in the extreme, the decay follows a power-law decay.[44] The time constants for the slowest decay were set to that found after fitting the decay of $[Tyr + H]^+$ when no photoexcitation occurred (CID decay). From a fit to the experimental data, it was possible to extrapolate back to time zero, defined as the time when the laser was fired, and sum the decay due to both decay channels for each wavelength used. Summing over the entire time of decay is important as changes in lifetimes with λ could significantly affect the calculated values of absorption if not calculated over the entire decay time from time zero. The resulting absorption spectrum for $[Tyr + H]^+$ in vacuo is shown in Figure 4B where it can be seen that there is one band which ranges from 210 nm, the lowest end of our scale, to ~255 nm, peaking at about 225 nm. The solution-phase spectrum is also included in the figure. In water, the first band maximum is at 222 nm, but the second band at 275 nm is absent from the gas-phase spectrum. Explanations for this are discussed below.

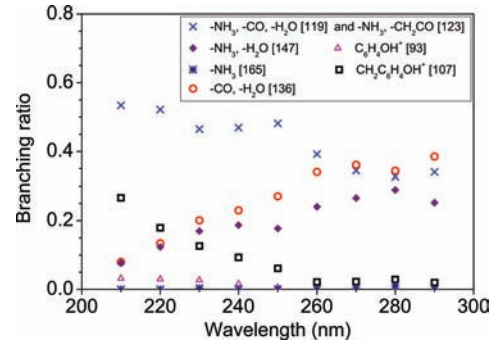

Figure 5. Branching ratios for fragmentation channels of $[Tyr + H]^+$ (*m/z* 182) as a function of excitation wavelength. The resolution is too low to separate *m/z* 119 and 123 so they are summed. The signal for each peak was divided by the mass to correct for sampling efficiency. Fragment ion masses are in brackets.

Photodissociation mass spectra of $[Tyr + H]^+$ (*m/z* 182) after excitation in the range 210−300 nm were also measured (for 220-nm absorption, see Figure 4C). Fragment ions formed in the time from 0 to 18 μs after photoexcitation were sampled. Peaks can be assigned to ions that have lost NH_3 (*m/z* 165), NH_3 and H_2O (*m/z* 147), CO and H_2O (*m/z* 136), NH_3 and CH_2CO (*m/z* 123), and NH_3, CO, and H_2O (*m/z* 119), and a peak which corresponds to the side chain ion (*m/z* 107). The observation of these peaks is in accordance with a previously reported spectrum by Kang et al.[25] recorded at 266 nm. In our spectrum there are two additional peaks at *m/z* 93 corresponding to $C_6H_4OH^+$ and at *m/z* 103, currently unassigned.

The branching ratios for the different fragment ions as a function of excitation wavelength are shown in Figure 5. It is evident that the *m/z*-107 peak decreases in importance with λ. This peak is a fingerprint for the formation of the tyrosine radical cation by hydrogen loss from photoexcited $[Tyr + H]^+$. As shown by Kang et al.,[25] a crossing from the initially reached $\pi\pi^*$ state on the phenol to the $\pi\sigma^*$ state on the ammonium occurs with about 25% probability after 266-nm photoexcitation. H loss requires 4.0 eV, and taking into account the fact that the hydrogen leaves with a significant amount of energy, the $Tyr^{+\bullet}$ radical cations have limited energy but a broad internal energy distribution as shown earlier in the case of tryptophan.[40] The side chain cation (*m/z* 107) is then formed from the $Tyr^{+\bullet}$ radical after $C_\alpha - C_\beta$ bond cleavage. Competing internal conversion from the $\pi\pi^*$ state back to the electronic ground state leads instead to hot $[Tyr + H]^+$ ions that dissociate with a time constant of less than 10 μs (see Figure 1).[45] In the present measurements, it is impossible to distinguish between $[Tyr + H]^+$ and $Tyr^{+\bullet}$ due to the poor mass resolution of the ring elements.

It is now possible to explain the absence of the 270-nm band in the action spectrum: Dissociation occurs over longer time periods when the ion has less energy; hence, further dissociation after hydrogen loss subsequent to 270-nm photoexcitation may not occur on the time scales investigated in the current experiments. In contrast, further dissociation after hydrogen loss following 220-nm photoexcitation is more probable due to the larger amounts of energy deposited. The photon energy at 270 nm is 4.6 eV, while it is more than 1 eV higher at 220 nm (5.7 eV), which would clearly have a noticeable effect on the lifetime of $Tyr^{+\bullet}$ ions. Consequently, absorption at 220 nm has been

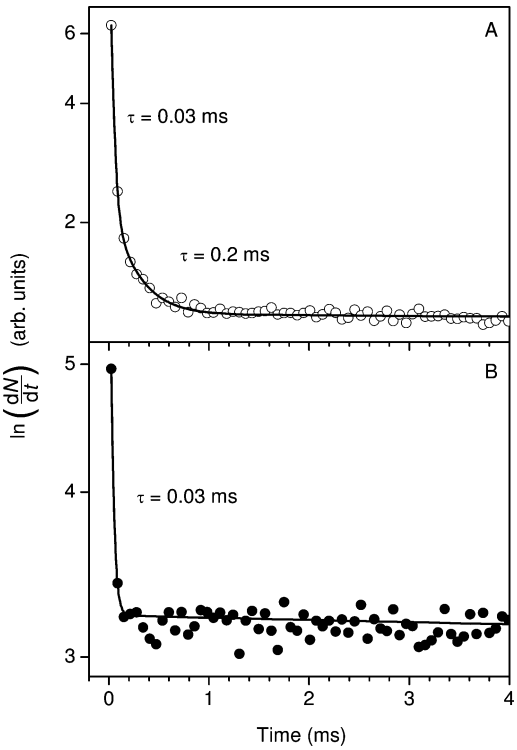

Figure 6. Time spectra of (A) [Ala-Tyr + H]$^+$ (*m*/*z* 253) and (B) [Tyr-Ala + H]$^+$ (*m*/*z* 253) after 220-nm photoexcitation. The solid curve in (A) is the fit of three exponentials to the data with one of the exponentials corresponding to the background decay (τ = 0.3 s). Lifetimes associated with the other decays are indicated on the graph. The solid curve in (B) is the fit of two exponentials to the data with one of the exponentials corresponding to the background decay (τ = 0.3 s). The lifetime associated with the other decay is indicated on the graph.

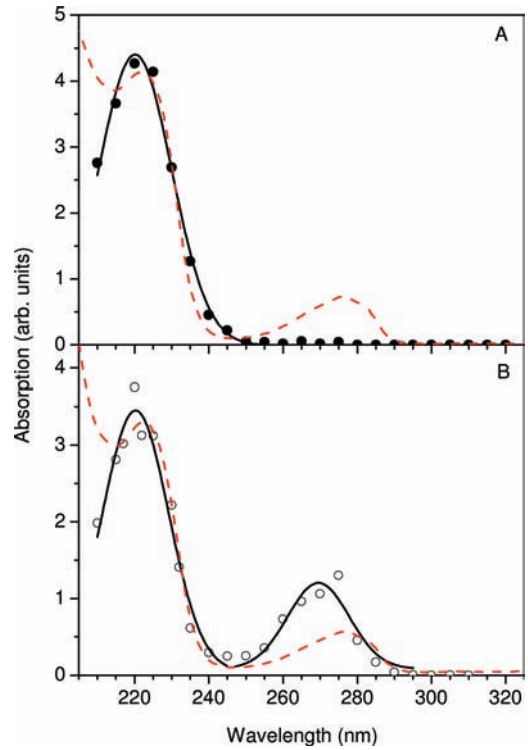

Figure 7. Absorption spectra of (A) [Ala-Tyr + H]$^+$ (*m*/*z* 253) and (B) [Ala-Tyr + H]$^+$(CE) (*m*/*z* 517) in vacuo. Gaussian fits to the data are shown as solid lines. Absorption spectra of solution-phase Ala-Tyr and Ala-Tyr(CE) are shown as red dashed lines. Addition of crown ether to the solution does not change the absorption.

measured, whereas absorption at 270 nm appears to be absent when the first neutrals sampled are formed after 27 μs. It should be mentioned that delayed dissociation has earlier been observed where photodissociation was achieved using the fourth harmonic light of a Nd:YAG laser (266 nm).[38] The light intensity was an order of magnitude higher than that in the present experiment, resulting in more photoexcited ions and consequently a higher yield of neutrals. We assume that it is only ions at the upper end of the internal energy distribution that have enough energy for dissociation. Another complication besides too few Tyr$^{+\bullet}$ ions dissociating at high wavelengths arises from the fact that the crossing to the $\pi\sigma^*(NH_3)$ state may depend strongly on excitation wavelength; hence, an action spectrum based on integration of the yield of all product ions, formed from 0 to 18 μs, not including Tyr$^{+\bullet}$ could also be incorrect.

Protonated Ala-Tyr and Tyr-Ala. Time spectra of [Ala-Tyr + H]$^+$ and [Tyr-Ala + H]$^+$ are shown in Figure 6 after 220-nm photoexcitation (initially sampling neutrals produced between 31 and 52 μs after photoexcitation, and then after successive rotations in the ring). Both ions dissociate with a time constant of 0.03 ms, which indicates that the dissociation channels are similar or that the activation energies and preexponential factors are. The better statistics in the spectrum for [Ala-Tyr + H]$^+$ reveals a tail to longer times that can be fit with an exponential associated with a time constant of 0.2 ms. The tail is a result of the width of the internal energy distribution; not all ions have exactly the same energy after photoexcitation. The experiment was repeated at higher wavelengths, 250−280 nm, but no photoinduced signal could be discerned from the background collision induced dissociation signal. Based on the lifetimes, we obtain the gas-phase absorption spectra shown in Figures 7A and 8A. For both peptides the band is at ∼220 nm, which is close to that obtained in water solution (Figures 7A and 8A). The band shapes are very similar for the solution- and gas-phase experiments. In addition, they are comparable to that measured for protonated tyrosine, which indicates that for the dipeptides the electronic transition is also due to excitation of the phenol ring.

We now describe the fragmentation channels for the two dipeptides. Photodissociation mass spectra of [Ala-Tyr + H]$^+$ recorded at excitation wavelengths of 210 and 270 nm are shown in Figure 9. Fragment ions formed from 0 to 21 μs after photoexcitation were sampled. At the highest wavelength, the largest peak corresponds to y^+ ions (*m*/*z* 180), whereas x^+ (*m*/*z* 208) or ions that have lost CO + H_2O (*m*/*z* 207) ions are formed dominantly at the low wavelength. Side chain cleavages also occur, with most at 220 nm. In accordance with this, the specific fragmentation of the $C_\alpha-C_\beta$ bond of the tyrosyl residue was observed to occur after 262-nm excitation of larger tyrosyl-containing peptides.[46,47] In our work, there is also a small signal due to loss of ammonia. The wavelength dependence of the different channels is presented in Figure 10A, where it is evident that the transition from y^+ to *m*/*z* 207/208 occurs gradually with decreasing λ.

The y^+ ions are expectedly formed after internal conversion to the electronic ground state since rupture of the peptide bond is a dominant channel in low-energy CID experiments. The fact that no delayed dissociation is observed at 270 nm then implies that the time constant for statistical dissociation is too short for the photoexcited parent ions to survive half a revolution in the ring (32 μs); the same is true for [Tyr-Ala + H]$^+$.

IR-UV double resonance spectroscopy of cold [Ala-Tyr + H]$^+$ ions by Stearns et al.[48,49] revealed a strong interaction

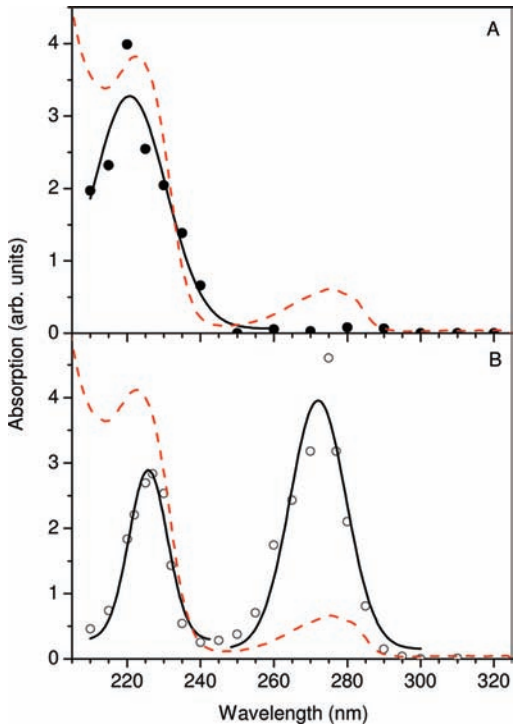

Figure 8. Absorption spectra of (A) $[Tyr\text{-}Ala + H]^+$ (m/z 253) and (B) $[Tyr\text{-}Ala + H]^+(CE)$ (m/z 517) in vacuo. Gaussian fits to the data are shown as solid lines. Absorption spectra of solution-phase Tyr-Ala and Tyr-Ala(CE) are shown as red dashed lines. Addition of crown ether to the solution does not change the absorption.

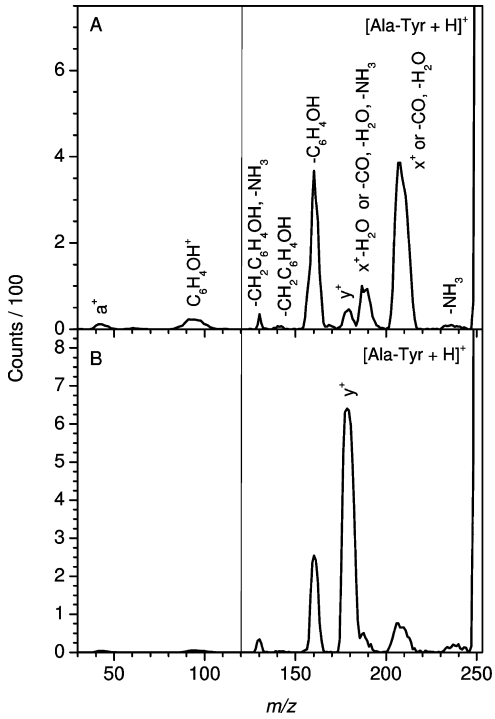

Figure 9. Photodissociation mass spectra of $[Ala\text{-}Tyr + H]^+$ (m/z 253) after (A) 210-nm and (B) 270-nm photoexcitation. The ions with m/z < 120 were dumped on the detector after 1.5 revolutions, while the ions with m/z > 120 were dumped on the detector after 7.5 revolutions.

between the ammonium group and the π cloud of the phenol; it is likely that some ions in such a structure are present in our ion beam (room temperature internal energy distribution). The high crossing probability to the $\pi\sigma^*(NH_3)$ state is then most likely due to the short distance the photoactive electron has to jump. The $\pi\sigma^*(NH_3)$ state may, however, efficiently couple with the ground state preventing hydrogen loss. For comparison, Gregoire et al.[24] found that while the $\pi\sigma^*$ state is populated in $[Gly\text{-}Tyr\text{-}Gly + H]^+$ after 266-nm photoexcitation, hydrogen loss did not occur. It was suggested that H loss would be suppressed by a kind of cage effect. In agreement with this, we have earlier shown that $[Lys\text{-}Tyr\text{-}Lys + H]^+$ after 266-nm photon absorption decays exponentially.[38] Finally, the suppression of H loss was observed in related experiments involving electron transfer from sodium atoms to peptide dications. In this work, all dipeptides studied lost hydrogen, whereas the intact charge-reduced cation was observed in high yield for tripeptides and larger peptides.[50] Solvation had a similar effect, namely, preventing hydrogen loss. Tabarin et al.,[46] however, found that the protonated leucine-enkephalin lost hydrogen at 220-nm excitation but not at 260 nm. In any case, ions that lose hydrogen at 277 nm will be too cold for subsequent dissociation, while the larger local energy depositions at 220 nm may lead to more hydrogen loss and radical cations that now dissociate on a time scale which is within the window of the experiment.

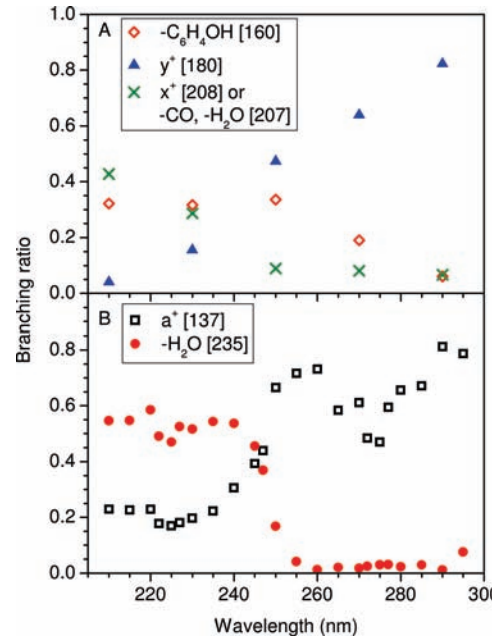

Figure 10. Branching ratios for the main fragmentation channels of (A) $[Ala\text{-}Tyr + H]^+$ and (B) $[Tyr\text{-}Ala + H]^+$ as a function of excitation wavelength. Fragmentation channels with branching ratios <10% are not included on the graphs for clarity but were included in the branching ratio calculations. The signal for each peak was divided by the mass to correct for sampling efficiency. Fragment ion masses are in brackets.

The corresponding photodissociation mass spectra of $[Tyr\text{-}Ala + H]^+$ are shown in Figure 11. Fragment ions were formed from 0 to 21 μs after photoexcitation. At both 210 and 270 nm, a^+ ions (Y immonium) (m/z 136) are formed with a high yield and $a^+\text{-}NH_3$ (m/z 120) with a minor yield. The a^+ fragment ion was also found to be dominant after 266-nm, 277-nm, and 284-nm photon excitation in ion traps reported by Gabryelski et al.,[51] Yoon et al.,[52] and Stearns et al.,[49] respectively. At the low wavelength, H_2O loss occurs to a large extent (m/z 235). This loss may be linked to the photoactive electron jumping to the carboxylic acid group and concomitant proton transfer to the negatively charged COOH group from ammonium, as described in the case of protonated tryptophan.[53] A wavelength dependent study (Figure 10B) reveals that water loss is dominant after

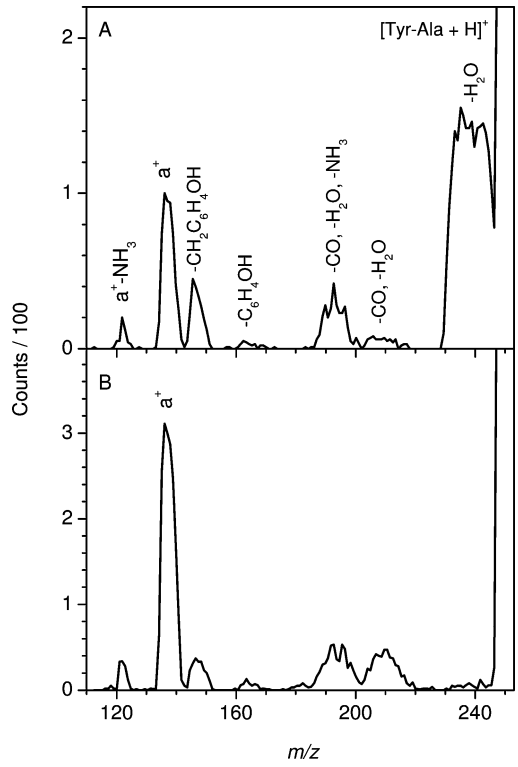

Figure 11. Photodissociation mass spectra of $[Tyr\text{-}Ala + H]^+$ (m/z 253) after (A) 210-nm and (B) 270-nm photoexcitation.

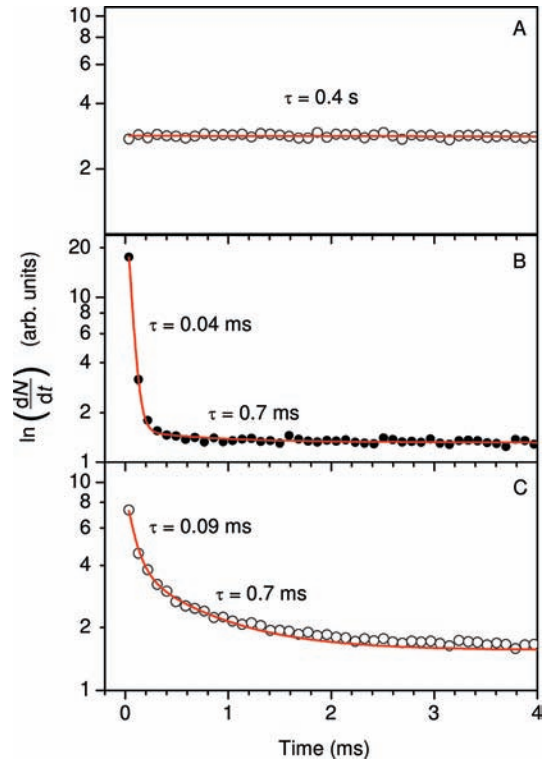

Figure 12. Time spectra of $[Ala\text{-}Tyr + H]^+$(CE) (m/z 517) after (A) no photoexcitation, (B) 220-nm photoexcitation, and (C) 270-nm photoexcitation. The lifetime associated with the exponential corresponding to the background was 0.4 s, which was found by fitting an exponential to the data in (A). The solid curves in (B) and (C) are fits of three exponentials to the data with one of the exponentials in both cases corresponding to the background decay. For (B) it was found that the lifetimes associated with the first two exponentials were 0.04 and 0.7 ms, while for (C) the lifetimes associated with the first two exponentials were 0.09 and 0.7 ms.

excitation within the 220-nm band whereas a^+ ions are formed in highest abundance after excitation within the 270-nm band; the transition between the two channels is quite abrupt at 245 nm. Side chain cleavages are also seen to take place as well as loss of CO and H_2O. Loss of the tyrosine side chain radical to give the fragment ion at m/z 146 has been attributed to dissociation from an excited electronic state of $[Tyr + H]^+$.[48] The distance between phenol and ammonium is assumed to be the same in $[Tyr\text{-}Ala + H]^+$ and $[Tyr + H]^+$, but H loss would again result in ions with too low an internal energy to give delayed formation of neutrals after 270-nm excitation.

To summarize the results for the bare ions, we have found that it is not possible to measure a 270-nm absorption band from delayed dissociation after half a revolution (at least not with the photon fluxes provided by our tunable laser system), which we have taken to be due to (i) the coupling between the $\pi\pi^*$(phenol) and $\pi\sigma^*(NH_3)$ states and subsequent hydrogen loss leaving ions with too low internal energy for further fragmentation and (ii) a too short lifetime of the parent ions after internal conversion back to the electronic ground state. Absorption does indeed happen in this wavelength region, which is evident from our photodissociation mass spectra (and from previous work by others), but we are blind to it in the delayed dissociation experiments. To circumvent this artifact of action spectroscopy, we decided to look at complexes between the dipeptide cations and crown ether. The latter targets the N-terminal ammonium group and raises the $\pi\sigma^*$ state up in energy, and most likely out of the spectral region even at the lowest wavelengths. In any case, the H-loss reaction is blocked. Second, the complex has more degrees of freedom and should as a result have a longer lifetime with respect to statistical dissociation. As we will show, the lifetime is also increased since the mobile proton mechanism that accounts for the facile breakage of peptide bonds[54,55] is no longer operative, which implies that the activation energy for dissociation is higher for the complex than for the bare ion itself.

Crown Ether Complexes. Sample time spectra for $[Ala\text{-}Tyr + H]^+$(CE) after no photoexcitation, 220-nm photoexcitation, and 270-nm photoexcitation are shown in Figure 12. Clearly, delayed dissociation (sampling neutrals formed between 46 and 77 μs after photoexcitation in the first instance, and then after successive rotations in the ring) is now also measured at the high wavelength, which is in support of our earlier interpretation for the absence of the peak in the bare ion spectra. Indeed, it was found that the time constants for the two decay processes increased as a function of wavelength, as expected for statistical dissociation processes. The spectra for $[Tyr\text{-}Ala + H]^+$(CE) (data not shown) were found to be similar to those for $[Ala\text{-}Tyr + H]^+$(CE). Based on the lifetime spectra and exponential fits to the data points, we have obtained the absorption spectra (Figures 7B and 8B). These display two absorption bands at 220 and 270 nm in the case of $[Ala\text{-}Tyr + H]^+$(CE) and at 226 and 272 nm in the case of $[Tyr\text{-}Ala + H]^+$(CE), with the second absorption band appearing to be larger than the first one for $[Tyr\text{-}Ala + H]^+$(CE). In fact, the ratio between the maxima of the 220 and 270 nm bands in both cases is smaller than that observed from the solution-phase spectra (Figures 7B and 8B). It should be mentioned though that the lifetimes after excitation at the low wavelengths are short and measured based on just two points which introduces some uncertainty when we calculate back to time zero to obtain the total number of photoexcited ions. Also fast dissociation from excited states may be more prominent at 220-nm excitation than at 270 nm, which results in some decay not being sampled at the lower wavelength. In previous work, Joly et al.[34,35] recorded the spectra of the doubly

TABLE 1: Absorption Spectra Band Maxima

	in vacuo	in aqueous solution
	λ_{max} (nm)	λ_{max} (nm)
$[Tyr + H]^+$	225	222, 275
$[Ala\text{-}Tyr + H]^+$	220	221, 276
$[Tyr\text{-}Ala + H]^+$	221	222, 275
$[Ala\text{-}Tyr + H]^+(CE)$	220, 270	222, 277
$[Tyr\text{-}Ala + H]^+(CE)$	226, 272	223, 275

negatively charged angiotensin II variant (DRVYVHPF) and DYKDDDDK peptides from photodetachment yields and found maximum absorption between 260 and 300 nm. Their spectra appear more to the red compared to ours, which may be linked to differences in the electric field at the tyrosine chromophore and the folding pattern. The solution-phase spectra of $[Ala\text{-}Tyr + H]^+(CE)$ and $[Tyr\text{-}Ala + H]^+(CE)$ are included in Figures 7 and 8. Our data reveal that solvation of the phenol chromophore by water has little influence. Thus, it is evident that water perturbs the high-energy transition by about 3 nm while the band at 270 nm red shifts by about 5 nm (Table 1). A similar pattern is expected when a tyrosine amino acid residue located in a hydrophobic pocket turns inside out and becomes solvated by water. This information may be useful for protein dynamics experiments that are based on either absorption or resonance Raman spectroscopy.

Photodissociation mass spectra of both $[Ala\text{-}Tyr + H]^+(CE)$ and $[Tyr\text{-}Ala + H]^+(CE)$ after 220-nm photoexcitation are shown in Figure 13, while the spectra obtained after 270-nm photoexcitation are shown in Figure 14. Product ions produced up to 31 μs after photoexcitation were sampled. The spectra are similar for both complexes and reveal that the dominant channel is loss of the tyrosine side chain (*m/z* 410). It is found that H_2O and CO losses increase in importance with higher

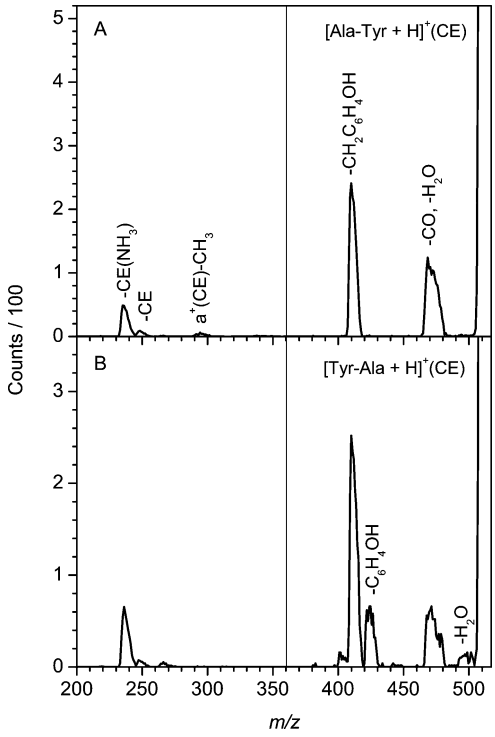

Figure 13. Photodissociation mass spectra of (A) $[Ala\text{-}Tyr + H]^+(CE)$ (*m/z* 517) and (B) $[Tyr\text{-}Ala + H]^+(CE)$ (*m/z* 517) after 220-nm photoexcitation. The ions with *m/z* < 360 were dumped on the detector after 1.5 revolutions, while the ions with *m/z* > 360 were dumped on the detector after 9.5 revolutions.

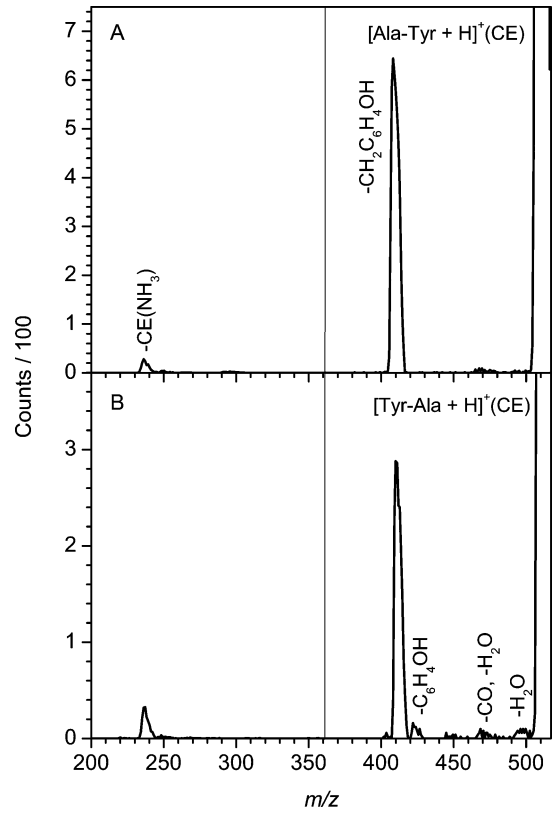

Figure 14. Photodissociation mass spectra of (A) $[Ala\text{-}Tyr + H]^+(CE)$ (*m/z* 517) and (B) $[Tyr\text{-}Ala + H]^+(CE)$ (*m/z* 517) after 270-nm photoexcitation. The ions with *m/z* < 360 were dumped on the detector after 1.5 revolutions, while the ions with *m/z* > 360 were dumped on the detector after 9.5 revolutions.

excitation energies. In the lower *m/z* region, there are peaks that correspond to fragments formed after loss of CE or CE and ammonia, with protonated crown ether also being measured. It is worthwhile to notice that no or very little fragmentation of the peptide backbone is seen to occur. For comparison, y^+ ions were formed in high yields after 270-nm photoexcitation of bare $[Ala\text{-}Tyr + H]^+$ ions. It is generally accepted that after vibrational heating of a peptide cation, the ionizing proton is no longer sequestered at the most basic site—in the case of $[Ala\text{-}Tyr + H]^+$ and $[Tyr\text{-}Ala + H]^+$, this is the N-terminal amino group—but is instead mobile and can explore less basic sites such as the amide nitrogens. Amide protonation weakens the C(O)−N bond and accounts for the formation of *y* and *b* fragments. In the complexes, however, crown ether firmly binds the ammonium protons[42] and reduces or prevents internal proton transfer reactions after excitation. Channels other than backbone cleavages, such as side chain losses, are then possible (see Figure 15).

Conclusions

In general, measurement of an action spectrum requires that ionic dissociation takes place within the relevant time window of the instrument. Complications arise when fast nonstatistical processes occur that may be highly wavelength dependent, e.g., hydrogen loss from neutralized ammonium groups. Dehydrogenated ions will have low internal energies, and in some cases the energy will be too low for subsequent dissociation to be recorded in a delayed dissociation experiment. To prevent hydrogen loss, we have introduced a scheme based on crown ether attachment to the ammonium group since this brings the $\pi\sigma^*$ state on ammonium outside the spectral region. The

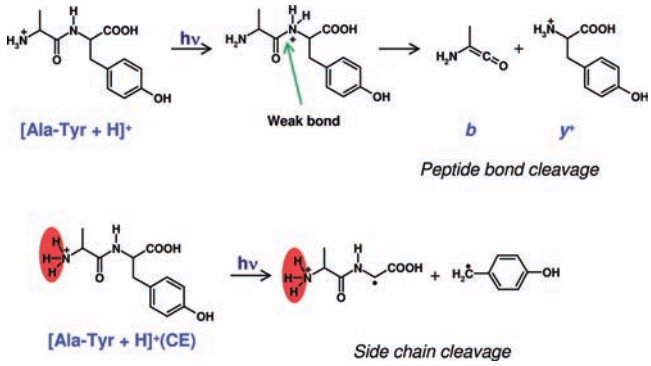

Figure 15. For the dipeptides, the ionizing proton is mobile. Breakage of the weakest bond forms *y* and *b* fragments, which is the dominant channel at high wavelengths in the case of [Ala-Tyr + H]$^+$. In the complexes, 18-crown-6 ether (indicated in red) prevents internal proton transfer after excitation. Channels other than backbone cleavages, such as side chain losses, are then possible.

photoactive electron instead duly jumps back to the electronic ground state (internal conversion) to give vibrationally hot ions that dissociate statistically. In this way, we succeeded in recording the gas-phase absorption spectra of the dipeptides [Ala-Tyr + H]$^+$(CE) and [Tyr-Ala + H]$^+$(CE) using an electrostatic ion storage ring. The spectra were obtained from measurements of the time decays as a function of excitation wavelength. The decays were to a good approximation exponential, which allowed us to estimate the initial number of photoexcited ions (relative numbers). In a ring experiment, we do not encounter the complication of kinetic shifts as seen in other instruments that rely on a finite time for sampling the fragments. The gas-phase absorption spectra of the two crown ether peptide complexes are very similar to those obtained in aqueous solution, which indicates that the environment only weakly perturbs the electronic transition energies. Absorption band maxima of all species under study are summarized in Table 1, from which it is evident that the band maxima are nearly the same for protonated Tyr, Ala-Tyr, and Tyr-Ala. This implies that the phenol group is the photoactive group at all wavelengths from 210 to 300 nm. Finally, we have reported photodissociation mass spectra as a function of excitation wavelength both for bare dipeptides and crown ether complexes. The latter are less prone to internal proton transfer after excitation, and as a result side chain cleavages take over from the backbone cleavages observed for the bare ions. Tagging ammonium groups by crown ether serves a dual purpose: it eliminates H loss and sequesters the protons.

Acknowledgment. We gratefully acknowledge support from Villum Kann Rasmussen fonden, Lundbeckfonden (Junior Group Leader Fellowship), Carlsbergfondet (grant 2006-01-0229), FNU (grant 272-06-0427), and Dir. Ib Henriksens Fond.

References and Notes

(1) Brøndsted Nielsen, S.; Lapierre, A.; Andersen, J. U.; Pedersen, U. V.; Tomita, S.; Andersen, L. H. *Phys. Rev. Lett.* **2001**, *87*, 228102.
(2) Andersen, L. H.; Nielsen, I. B.; Kristensen, M. B.; El Ghazaly, M. O. A.; Haacke, S.; Brøndsted Nielsen, M.; Petersen, M. Å. *J. Am. Chem. Soc.* **2005**, *127*, 12347.
(3) Nielsen, I. B.; Lammich, L.; Andersen, L. H. *Phys. Rev. Lett.* **2006**, *96*, 018304.
(4) Lykkegaard, M. K.; Ehlerding, A.; Hvelplund, P.; Kadhane, U.; Kirketerp, M. B. S.; Brøndsted Nielsen, S.; Panja, S.; Wyer, J. A.; Zettergren, H. *J. Am. Chem. Soc.* **2008**, *130*, 11856.
(5) Kirketerp, M.-B. S.; Petersen, M. Å.; Wanko, M.; Leal, L. A. E.; Zettergren, H.; Raymo, F. M.; Rubio, A.; Brøndsted Nielsen, M.; Brøndsted Nielsen, S. *Chem. Phys. Chem.* **2009**, *10*, 1207.
(6) Marques, M. A. L.; Gross, E. K. U. *Annu. Rev. Phys. Chem.* **2004**, *55*, 427.
(7) Olsen, S.; Smith, S. C. *J. Am. Chem. Soc.* **2007**, *129*, 2054.
(8) Patnaik, S. S.; Trohalaki, S.; Naik, R. R.; Stone, M. O.; Pachter, R. *Biopolymers* **2007**, *85*, 253.
(9) Altoe, P.; Stenta, M.; Bottoni, A.; Garavelli, M. *Theor. Chem. Acc.* **2007**, *118*, 219.
(10) Hasegawa, J. Y.; Fujimoto, K.; Swerts, B.; Miyahara, T.; Nakatsuji, H. *J. Comput. Chem.* **2007**, *28*, 2443.
(11) Send, R.; Sundholm, D. *Phys. Chem. Chem. Phys.* **2007**, *9*, 2862.
(12) Wanko, M.; Hoffmann, M.; Frauenheim, T.; Elstner, M. *J. Phys. Chem. B* **2008**, *112*, 11462.
(13) Soderhjelm, P.; Husberg, C.; Strambi, A.; Olivucci, M.; Ryde, U. *J. Chem. Theory Comput.* **2009**, *5*, 649.
(14) Møller, S. P. *Nucl. Instrum. Methods Phys. Res., Sect. A* **1997**, *394*, 281.
(15) Andersen, J. U.; Hvelplund, P.; Brøndsted Nielsen, S.; Tomita, S.; Wahlgreen, H.; Møller, S. P.; Pedersen, U. V.; Forster, J. S.; Jørgensen, T. J. D. *Rev. Sci. Instrum.* **2002**, *73*, 1284.
(16) Støchkel, K.; Kadhane, U.; Andersen, J. U.; Holm, A. I. S.; Hvelplund, P.; Kirketerp, M. B. S.; Larsen, M. K.; Lykkegaard, M. K.; Brøndsted Nielsen, S.; Panja, S.; Zettergren, H. *Rev. Sci. Instrum.* **2008**, *79*, 023107.
(17) Harada, I.; Takeuchi, H. Raman and Ultraviolet Resonance Raman Spectra of Proteins and Related Compounds. In *Spectroscopy of Biological Systems*; Clark, R. J. H., Hester, R. E., Eds.; John Wiley & Sons Ltd.: New York, 1986.
(18) Tabarin, T.; Kulesza, A.; Antoine, R.; Mitric, R.; Broyer, M.; Dugourd, P.; Bonacic-Koutecky, V. *Phys. Rev. Lett.* **2008**, *101*, 213001.
(19) Weinkauf, R.; Schanen, P.; Metsala, A.; Schlag, E. W.; Burgle, M.; Kessler, H. *J. Phys. Chem.* **1996**, *100*, 18567.
(20) Weinkauf, R.; Schlag, E. W.; Martinez, T. J.; Levine, R. D. *J. Phys. Chem. A* **1997**, *101*, 7702.
(21) Hu, Y. J.; Hadas, B.; Davidovitz, M.; Balta, B.; Lifshitz, C. *J. Phys. Chem. A* **2003**, *107*, 6507.
(22) Cui, W.; Hu, Y.; Lifshitz, C. *Eur. Phys. J. D* **2002**, *20*, 565.
(23) Armentrout, P. B. Threshold Collision-Induced Dissociations for the Determination of Accurate Gas-Phase Binding Energies and Reaction Barriers. In *Modern Mass Spectrometry*; Springer-Verlag: Berlin, 2003; Vol. 225; p 233.
(24) Gregoire, G.; Dedonder-Lardeux, C.; Jouvet, C.; Desfrancois, C.; Fayeton, J. A. *Phys. Chem. Chem. Phys.* **2007**, *9*, 78.
(25) Kang, H.; Jouvet, C.; Dedonder-Lardeux, C.; Martrenchard, S.; Gregoire, G.; Desfrancois, C.; Schermann, J. P.; Barat, M.; Fayeton, J. A. *Phys. Chem. Chem. Phys.* **2005**, *7*, 394.
(26) Boyarkin, O. V.; Mercier, S. R.; Kamariotis, A.; Rizzo, T. R. *J. Am. Chem. Soc.* **2006**, *128*, 2816.
(27) Fujihara, A.; Matsumoto, H.; Shibata, Y.; Ishikawa, H.; Fuke, K. *J. Phys. Chem. A* **2008**, *112*, 1457.
(28) Yoon, S. H.; Kim, M. S. *J. Am. Soc. Mass Spectrom.* **2007**, *18*, 1729.
(29) Oh, J. Y.; Moon, J. H.; Kim, M. S. *J. Mass Spectrom.* **2005**, *40*, 899.
(30) Nolting, D.; Schultz, T.; Hertel, I. V.; Weinkauf, R. *Phys. Chem. Chem. Phys.* **2006**, *8*, 5247.
(31) Weinkauf, R.; Schanen, P.; Yang, D.; Sonkara, S.; Schlag, E. W. *J. Phys. Chem.* **1995**, *99*, 11255.
(32) Sobolewski, A. L.; Shemesh, D.; Domcke, W. *J. Phys. Chem. A* **2009**, *113*, 542.
(33) Cohen, R.; Brauer, B.; Nir, E.; Grace, L.; de Vries, M. S. *J. Phys. Chem. A* **2000**, *104*, 6351.
(34) Joly, L.; Antoine, R.; Allouche, A. R.; Broyer, M.; Lemoine, J.; Dugourd, P. *J. Am. Chem. Soc.* **2007**, *129*, 8428.
(35) Joly, L.; Antoine, R.; Broyer, M.; Lemoine, J.; Dugourd, P. *J. Phys. Chem. A* **2008**, *112*, 898.
(36) Kang, H.; Dedonder-Lardeux, C.; Jouvet, C.; Martrenchard, S.; Gregoire, G.; Desfrancois, C.; Schermann, J. P.; Barat, M.; Fayeton, J. A. *Phys. Chem. Chem. Phys.* **2004**, *6*, 2628.
(37) Lepere, V.; Lucas, B.; Barat, M.; Fayeton, J. A.; Picard, V. J.; Jouvet, C.; Carcabal, P.; Nielsen, I.; Dedonder-Lardeux, C.; Gregoire, G.; Fujii, A. *J. Chem. Phys.* **2007**, *127*, 134313.
(38) Andersen, J. U.; Cederquist, H.; Forster, J. S.; Huber, B. A.; Hvelplund, P.; Jensen, J.; Liu, B.; Manil, B.; Maunoury, L.; Brøndsted Nielsen, S.; Pedersen, U. V.; Rangama, J.; Schmidt, H. T.; Tomita, S.; Zettergren, H. *Phys. Chem. Chem. Phys.* **2004**, *6*, 2676.
(39) Holm, A. I. S.; Larsen, M. K.; Panja, S.; Hvelplund, P.; Brøndsted Nielsen, S.; Leib, R. D.; Donald, W. A.; Williams, E. R.; Hao, C. T.; Turecek, F. *Int. J. Mass Spectrom.* **2008**, *276*, 116.
(40) Kadhane, U.; Andersen, J. U.; Ehlerding, A.; Hvelplund, P.; Kirketerp, M. B. S.; Lykkegaard, M. K.; Brøndsted Nielsen, S.; Panja, S.; Wyer, J. A.; Zettergren, H. *J. Chem. Phys.* **2008**, *129*, 184304.
(41) Raevsky, O. A.; Solovev, V. P.; Solotnov, A. F.; Schneider, H. J.; Rudiger, V. *J. Org. Chem.* **1996**, *61*, 8113.

(42) Julian, R. R.; Beauchamp, J. L. *Int. J. Mass Spectrom.* **2001**, *210*, 613.

(43) Wilson, J. J.; Kirkovits, G. J.; Sessler, J. L.; Brodbelt, J. S. *J. Am. Soc. Mass Spectrom.* **2008**, *19*, 257.

(44) Andersen, J. U.; Cederquist, H.; Forster, J. S.; Huber, B. A.; Hvelplund, P.; Jensen, J.; Liu, B.; Manil, B.; Maunoury, L.; Brøndsted Nielsen, S.; Pedersen, U. V.; Schmidt, H. T.; Tomita, S.; Zettergren, H. *Eur. Phys. J. D* **2003**, *25*, 139.

(45) Fayeton, J. A.; et al. Personal communication.

(46) Tabarin, T.; Antoine, R.; Broyer, M.; Dugourd, P. *Rapid Commun. Mass Spectrom.* **2005**, *19*, 2883.

(47) Joly, L.; Antoine, R.; Broyer, M.; Dugourd, P.; Lemoine, J. *J. Mass Spectrom.* **2007**, *42*, 818.

(48) Stearns, J. A.; Mercier, S.; Seaiby, C.; Guidi, M.; Boyarkin, O. V.; Rizzo, T. R. *J. Am. Chem. Soc.* **2007**, *129*, 11814.

(49) Stearns, J. A.; Guidi, M.; Boyarkin, O. V.; Rizzo, T. R. *J. Chem. Phys.* **2007**, *127*, 154322.

(50) Chakraborty, T.; Holm, A. I. S.; Hvelplund, P.; Brøndsted Nielsen, S.; Poully, J. C.; Worm, E. S.; Williams, E. R. *J. Am. Soc. Mass Spectrom.* **2006**, *17*, 1675.

(51) Gabryelski, W.; Li, L. *Rev. Sci. Instrum.* **1999**, *70*, 4192.

(52) Yoon, T. O.; Choi, C. M.; Kim, H. J.; Kim, N. J. *Bull. Korean Chem. Soc.* **2007**, *28*, 619.

(53) Lucas, B.; Barat, M.; Fayeton, J. A.; Perot, M.; Jouvet, C.; Gregoire, G.; Brøndsted Nielsen, S. *J. Chem. Phys.* **2008**, *128*, 164302.

(54) Wysocki, V. H.; Tsaprailis, G.; Smith, L. L.; Breci, L. A. *J. Mass Spectrom.* **2000**, *35*, 1399.

(55) Wysocki, V. H.; Resing, K. A.; Zhang, Q. F.; Cheng, G. L. *Methods* **2005**, *35*, 211.

JP904053D